Single-Crystal ^{27}Al NMR Study of Corundum α-Al_2O_3

Ae Ja Woo

Department of Science Education, Ewha Womans University, Seoul 120-750, Korea
Received April 16, 1999

^{27}Al NMR chemical shielding, quadrupolar coupling, and dipolar coupling interactions for corundum (α-Al_2O_3) are determined from the single-crystal ^{27}Al NMR spectra according to the rotation about three orthogonal axis. ^{27}Al NMR parameters obtained in this work with high accuracy are as follows: δ_{iso} = 7.4(4) ppm, QCC = 2.30(4) MHz, η = 0.08(3), and R = 2.0(3) kHz. This work appears to be the first NMR measurement of an aluminum-aluminum dipolar coupling interaction in α-Al_2O_3 crystals.

Introduction

The critical feature of solid-state NMR spectroscopy is the preservation of the anisotropic character of spin interactions such as chemical shielding, dipolar coupling, and quadrupolar interactions due to the relatively fixed orientations of the molecules with respect to the applied magnetic field. In the case of quadrupolar nuclei ($I \geq 1$), the solid-state NMR spectra are dominated by the quadrupolar interaction. Therefore it is difficult to detect the chemical shielding and dipolar coupling interactions. Nevertheless, even in lighter quadrupolar nuclei, chemical shielding and dipolar coupling interactions cannot be neglected in the spectral interpretation. Single-crystal NMR[1-4] offers the most direct method with high accuracy to determine the magnitude and relative orientations of these NMR interactions.

α-Al_2O_3 crystals are widely utilized in microelectronics and catalysis[5] because of their hard, inert, and microporous properties. According to the ^{27}Al NMR studies of α-Al_2O_3, the octahedral aluminum site is identified as a single peak positioned in the range of 5 ppm to 20 ppm.[6-9] Single-crystal ^{27}Al NMR, SQUID, and NQR studies[6,7,10,11] provide the quadrupolar coupling constant and the asymmetry parameter of ~2.4 MHz and ~0, respectively. The aluminum-aluminum dipolar coupling interaction was not measured.

In this work, I attempt to obtain the ^{27}Al NMR chemical shielding, quadrupolar coupling, and dipolar coupling tensors for corundum by using single-crystal ^{27}Al NMR spectroscopy. For the aluminum site, the isotropic chemical shift δ_{iso}, quadrupolar coupling constant QCC, and asymmetry parameter η, and aluminum-aluminum dipolar coupling constant R are determined.

Theory

The total Hamiltonian governing the NMR spectrum of a quadrupolar nucleus is composed of the chemical shielding, the quadrupolar coupling, and the dipolar coupling interactions:

$$H_T = H_{CS} + H_Q + H_D \tag{1}$$

where the chemical shielding interaction[12] is given by

$$H_{CS} = -\omega_0(1-\sigma)I \tag{2}$$

and where ω_0 and I are the Larmor frequency and nuclear spin angular momentum operator, respectively. The chemical shielding tensor σ is a second-rank tensor with nine elements. In the principal axis system, the convention used for the relative assignment of the principal components of the chemical shielding tensor is $\sigma_{11} \geq \sigma_{22} \geq \sigma_{33}$. The isotropic chemical shift and the chemical shielding symmetry are represented by $\sigma_{iso} = 1/3(\sigma_{11}+\sigma_{22}+\sigma_{33})$ and $\eta_\sigma = (\sigma_{22}-\sigma_{11})/(\sigma_{iso}-\sigma_{11})$, respectively. The relation between σ- and δ-chemical shift scale is $\delta \approx -\sigma$.

The quadrupolar coupling interaction[12,13] is given by

$$H_Q = \frac{eQ}{2I(2I-1)\hbar} IVI \tag{3}$$

where Q and $V(=eq)$ are the nuclear quadrupole moment and the electric field gradient. The electric field gradient in the principal axis system can be described as a symmetric traceless tensor with the convention $|eq_{11}| \geq |eq_{22}| \geq |eq_{33}|$. The magnitude of the electric field gradient tensor is given by the quadrupole coupling constant, $QCC = e^2q_{11}Q/\hbar$. The deviation from axial symmetry is indicated by the asymmetry parameter, $\eta = (eq_{22}-eq_{33})/eq_{11}$ $(0 \leq \eta \leq 1)$. The electric field gradient tensor can be reduced to two parameters, eq_{11} and η:

$$V = -eq_{11}\begin{bmatrix} (1-\eta)/2 & 0 & 0 \\ 0 & (1+\eta)/2 & 0 \\ 0 & 0 & -1 \end{bmatrix} \tag{4}$$

The dipolar coupling interaction[14] is given by

$$H_D = I_1 D I_2 \tag{5}$$

where I_1 are I_2 the spin angular momentum operators of the nuclei 1 and 2. The dipolar coupling tensor D shows axially symmetric and traceless properties. In the principal axis system, D is described as

$$D = \begin{bmatrix} D_{11} & 0 & 0 \\ 0 & D_{22} & 0 \\ 0 & 0 & D_{33} \end{bmatrix} = \frac{2}{3}\Delta D \begin{bmatrix} 1/2 & 0 & 0 \\ 0 & 1/2 & 0 \\ 0 & 0 & -1 \end{bmatrix} \tag{6}$$

The anisotropy ΔD is given by

$$\frac{2}{3}\Delta D = \frac{2}{3}(D_{11} - D_{33}) = R \quad (7)$$

where the dipolar coupling constant $R = (\sqrt{3I(I+1)}/2)\omega_{ij}(1-3\cos^2\theta)$[15] and where the dipolar frequency $\omega_{ij} = \gamma_i\gamma_j\hbar/r^3$. Detecting the dipolar coupling interaction can be difficult because of the weak interaction relative to the chemical shielding and the quadrupolar interactions and the large line widths.

Experimental Section

Solid-state ^{27}Al NMR spectra for corundum α–Al_2O_3 crystal were acquired on a DSX400 solid-state NMR spectrometer operating at 104.3 MHz. A single-crystal goniometer NMR probe made by Bruker was used. The mounted crystal was rotated in 10° increments from 0 to 180° about three orthogonal axes (i = X, Y, and Z).[16,17] The 90° pulse length was 1 μs, and the spectra were acquired as simple Bloch decays. The relaxation delay was 20 s; spin-lattice relaxation times (T_1) for the central and inner-satellite transition peaks were measured to be 5.5 s and 0.013 s, respectively. Each spectrum was obtained by averaging 4 free induction decays, Fourier-transforming, and manual-phasing. The ^{27}Al NMR chemical shift values recorded on the δ-scale are referenced through external $Al(H_2O)_6^{3+}$ solution at 0 ppm.

Results and Discussion

In Figure 1, the energy level diagram of a spin I = 5/2 system (^{17}O, ^{27}Al, ^{55}Mn, ^{67}Zn, etc) shows six energy levels and

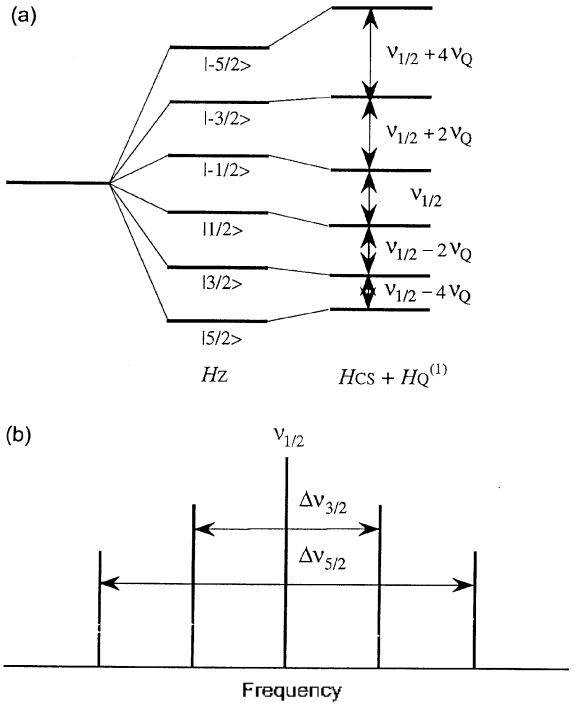

Figure 1. (a) The energy level diagram of a spin I = 5/2 system and (b) the resulting single-crystal NMR spectrum.

the resulting single-crystal NMR spectrum comprises five single quantum transitions. The central transition peak position $\upsilon_{1/2}$ is affected by the chemical shielding and the negligible second-order quadrupolar interaction. Splittings between symmetric satellite peaks $\Delta\upsilon_{3/2}$ and $\Delta\upsilon_{5/2}$ are affected only by the first-order quadrupolar interaction. If the dipolar coupling interaction were observable, the central and satellite transition peaks would show a split into the doublets, according to the magnitude of the dipolar coupling constant. Figure 2 shows the single-crystal ^{27}Al NMR spectra for corundum as a function of the orientation of the crystal in the external magnetic field. Rotations were performed in 10° increments about an axis perpendicular to the magnetic field directed along the X, Y, and Z axis.

Figure 3 shows the rotation plots, illustrating the ^{27}Al NMR chemical shielding (a), quadrupolar splitting (b), and dipolar splitting (c) for corundum as a function of the rotation angle φ. The positions of doublet peaks are determined by averaging the splitting frequency. The experimental data drawn for three axes i = X(●), Y(◆), and Z(■) are fitted to Eqn. (8) and nine coefficients A_i, B_i, and C_i are extracted by using a Simplex search method.

$$\upsilon(\varphi_i) = A_i + B_i\cos 2\varphi + C_i\sin 2\varphi \quad (8)$$

The values of chemical shielding on the δ-scale in Figure 3(a) are obtained from the central transition peaks. The chemical shielding tensor in the laboratory axis system can be constructed by using Eqn. (9);[16,17]

$$\begin{aligned}
\delta_{XX} &= (A_Y - B_Y - A_Z + B_Z)/2 \\
\delta_{YY} &= (A_Z - B_Z + A_X + B_X)/2 \\
\delta_{ZZ} &= (A_X - B_X + A_Y + B_Y)/2 \\
\delta_{XY} &= \delta_{YX} = -C_Z \\
\delta_{XZ} &= \delta_{ZX} = -C_Y \\
\delta_{YZ} &= \delta_{ZY} = -C_X
\end{aligned} \quad (9)$$

The quadrupolar splitting frequency in Figure 3(b) is acquired from Eqn. (10) based on the equation $\upsilon_Q = 3e^2q_{11}Q/$

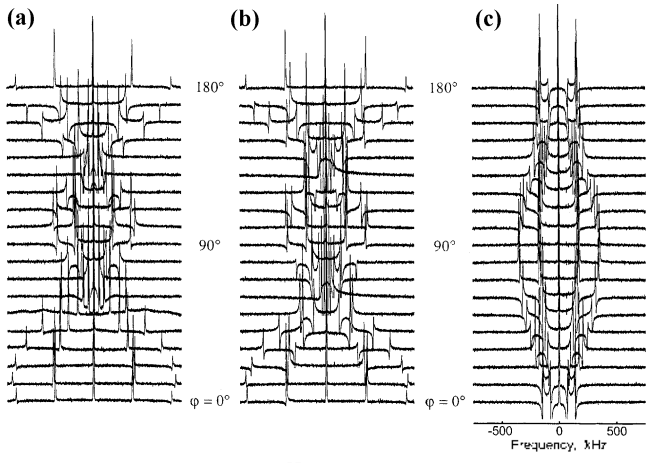

Figure 2. The single-crystal ^{27}Al NMR spectra of corundum as a function of the orientation of the crystal in the external magnetic field. Rotations were performed in 10° increments about an axis perpendicular to the magnetic field directed along the X (a), Y (b), and Z axis (c).

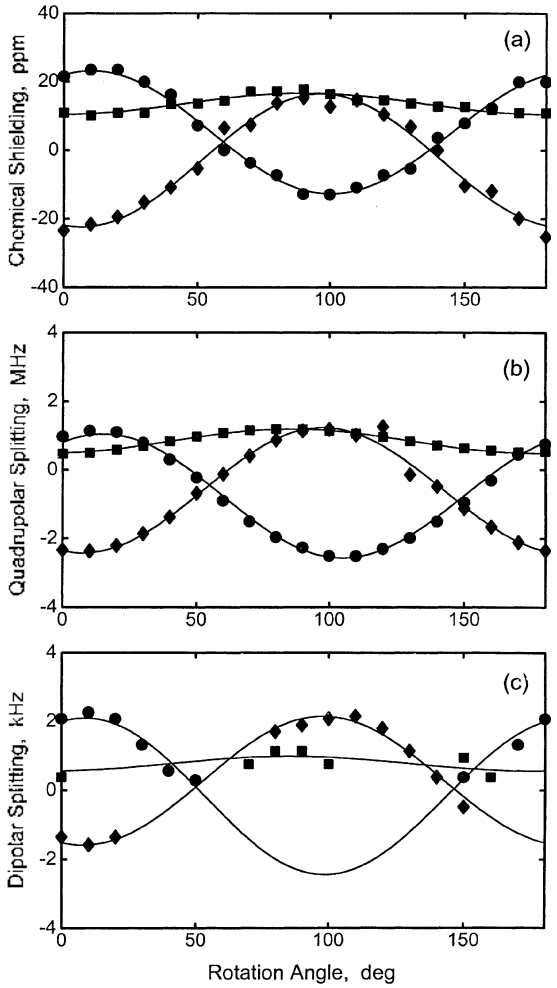

Figure 3. The rotation plots for corundum α-Al_2O_3 crystal illustrating (a) the ^{27}Al NMR chemical shielding, (b) quadrupolar splitting, and (c) dipolar splitting as a function of the rotation angle about three orthogonal axes. The experimental data are represented as circles (●), diamonds (◆), and squares (■) for three orthogonal axes *i* X, Y, and Z, respectively. The curves are calculated with the best fitted parameters.

$8I(2I-1)\hbar$ $(3\cos^2\theta-1+\eta\sin^2\theta\cos^2\phi)$, in which the maximum splitting of $\Delta\upsilon_{3/2}$ occurs when the magnetic field vector lies along eq_{11} of the electric field gradient tensor;

$$e^2q_{11}Q(\varphi_i)/\hbar = \frac{10}{3}\Delta\upsilon_{3/2} \tag{10}$$

where $\Delta\upsilon_{3/2}$ is the frequency difference between inner-satellite transition peaks. The dipolar splitting frequency in Figure 3(c) is equal to half the splitting frequency of the central transition peak. Splitting into the doublets is not always observable, so fewer experimental data points are shown in Figure 3(c). Due to the symmetric and traceless properties of the quadrupolar coupling and the dipolar coupling tensors, the tensor elements in Eqn. (9) can be modified as follows;

$$\begin{aligned} T_{XX} &= (-2A_X - A_Y - B_Y + A_Z - B_Z)/3 \\ T_{YY} &= (-2A_Y + A_Z - B_Z + A_X + B_X)/3 \\ T_{ZZ} &= (-2A_Z + A_X - B_X - A_Y + B_Y)/3 \\ T_{XY} &= T_{YX} = -C_Z \\ T_{XZ} &= T_{ZX} = -C_Y \\ T_{YZ} &= T_{ZY} = -C_X \end{aligned} \tag{11}$$

Employing the same procedure used for chemical shielding tensor, we constructed quadrupolar coupling and dipolar coupling tensors in the laboratory axis system by using Eqns. (8) and (11).

The principal elements of chemical shielding, quadrupolar coupling, and dipolar coupling tensors obtained by diagonalization with cosine directions are listed in Table 1. ^{27}Al NMR isotropic chemical shift δ_{iso} = 7.4(4) ppm is calculated from the chemical shielding tensor. In addition, from the quadrupolar coupling tensor, ^{27}Al NMR quadrupolar coupling constant QCC = 2.30(4) MHz and quadrupolar asymmetry parameter η = 0.08(3) are calculated. The values of δ_{iso}, QCC, and η are in good agreement with previously reported values at Table 2.

To confirm whether the doublets resulted from the aluminum-aluminum dipolar coupling or two sites of aluminum in

Table 1. Principal Components and Direction Cosines of the ^{27}Al NMR Chemical Shielding, Quadrupolar Coupling, and Dipolar Coupling Tensors for Corundum

Chemical Shielding (ppm)			Quadrupolar Coupling (MHz)			Dipolar Coupling (kHz)		
δ_{11}	δ_{22}	δ_{33}	$e^2q_{11}Q/\hbar$	$e^2q_{22}Q/\hbar$	$e^2q_{33}Q/\hbar$	D_{11}	D_{22}	D_{33}
-3.7(7)	0.8(4)	25.1(11)	-2.29(8)	1.24(8)	1.04(1)	1.0(2)	1.0(2)	-2.0(2)
0.952	-0.265	-0.151	-0.136	-0.089	0.185	-0.891	-0.453	0.009
-0.219	-0.939	0.267	0.152	-0.986	0.969	-0.439	0.869	0.228
0.213	0.221	0.952	0.979	0.141	-0.165	0.111	-0.199	0.974

Table 2. ^{27}Al Chemical Shielding, Quadrupolar Coupling, and Dipolar Coupling Parameters for α-Al_2O_3

Sample	Method	δ_{iso} (ppm)	QCC (MHz)	η	R (kHz)	ref.
Corundum	SC NMR	7.4(4)	2.30(4)	0.08(3)	2.0(3)	this work
Sapphire	SC NMR	18.8(3)	2.403(15)	0.009(13)	–	6
Corundum	NQR	–	2.4031(2)	0.0	–	7
powder α-Al_2O_3	MQMAS NMR	14(1)	2.38(5)	–	–	8

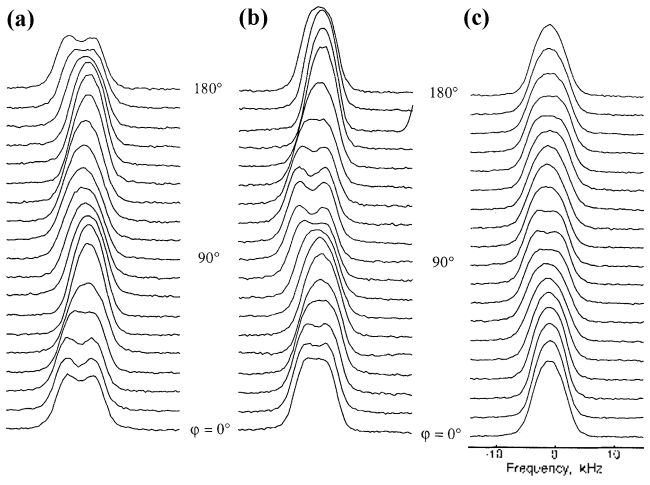

Figure 4. The central transition peaks obtained from the single-crystal ^{27}Al NMR spectra of corundum. Rotations were performed in 10° increments about an axis perpendicular to the magnetic field directed along the X (a), Y (b), and Z axis (c).

corundum, the two rotation plots acquired at 4.7 Tesla and 9.4 Tesla were compared, and they show exactly the same rotation patterns. This work appears to be the first NMR measurement of the aluminum-aluminum dipolar coupling interaction for α-Al_2O_3 crystals. Figure 4 was obtained by expanding the region of the central transition peak to show the dipolar splitting patterns. The relatively large deviation between experimental data and calculated fit may be due to the large Hz per point in the spectra. The dipolar coupling constant R and the dipolar frequency ω_D obtained from the dipolar coupling tensor D are 2.0(3) kHz and 429 Hz, respectively, which agrees well with 431 Hz calculated from the separation distance for aluminum, 2.66 Å.[18]

Dipolar coupling tensor can be used to find the major orientations of the chemical shielding and quadrupolar coupling tensors with respect to the molecular coordinate system by using the direction cosines listed in Table 1. The relative orientations of δ_{33} and eq_{11} with respect to the aluminum-aluminum bond axis are 4.7° and 1.3°, respectively, which means that the axes for three principal elements δ_{33}, eq_{11}, and D_{33} are nearly parallel.

Acknowledgment. This work was partially supported by Faculty Research Grant (1997) funded by Ewha Womans University. Korea Basic Science Institute is acknowledged here for the use of their Bruker MSL200 and DSX400 solid-state NMR spectrometers.

References

1. Eichele, K.; Chan, J. C. C.; Wasylishen, R. E.; Britten, *J. F. J. Phys. Chem. A* **1997**, *101*, 5423.
2. Kroeker, S.; Eichele, K.; Wasylishen, R. E.; Britten, J. F. *J. Phys. Chem. B* **1997**, *101*, 3727.
3. Vosegaard, T.; Massiot, D.; Gautier, N.; Jakobsen, H. J. *Inorg. Chem.* **1997**, *36*, 2446.
4. Vosegaard, T.; Skibsted, J.; Bilds, H.; Jakobsen, H. J. *J. Magn. Reson. A* **1996**, *122*, 111.
5. Yan, Y.; Tsapatsis, M.; Gavalas, G. R.; Davis, M. E. *J. Chem. Soc., Chem. Commun.* **1995**, 227.
6. Vosegaard, T.; Jakobsen, H. J. *J. Magn. Reson.* **1997**, *128*, 135.
7. Filsinger, B.; Gutsche, P.; Haeberlen, U.; Weiden, N. *J. Magn. Reson.* **1997**, *125*, 280.
8. Kraus, H.; Prins, R.; Kentgens, A. P. M. *J. Phys. Chem.* **1996**, *100*, 16336.
9. Carduner, K. R. *J. Magn. Reson.* **1989**, *81*, 312.
10. Chang, J.; Connor, C.; Hahn, E. L.; Huber, H.; Pines, A. *J. Magn. Reson.* **1989**, *82*, 387.
11. Gravina, S. J.; Bray, P. J. *J. Magn. Reson.* **1990**, *89*, 515.
12. Gerstein, B. C.; Dybowski, C. R. *Transient Techniques in NMR of Solids*; Academic Press: New York, 1985.
13. Mehring, M. *High Resolution NMR of Solids*, 2nd ed.; Springer-Verlag: Berlin, 1983.
14. Grimmer, A.-R.; Blumich, B. *Solid-State NMR I Methods*; Springer-Verlag: Berlin, 1994.
15. Lacelle, S.; Tremblay, L. *J. Chem. Phys.* **1993**, *98*, 3642.
16. Kennedy, M. A.; Ellis, P. D. *Concepts Magn. Res.* **1989**, *1*, 35.
17. Kennedy, M. A.; Ellis, P. D. *Concepts Magn. Res.* **1989**, *1*, 109.
18. Ishizawa, N.; Miyata, T.; Minato, I.; Marumo, F.; Iwai, S. *Acta Cryst.* **1980**, *B36*, 228.